Increasing ductility in heavily reinforced LWAC structures

Jan A. Øverli[a,1] and Tore Myrland Jensen[b]

[a]Department of Structural Engineering, Norwegian University of Science and Technology, NO-7491 Trondheim, Norway, E-mail: jan.overli@ntnu.no, Tel: +47 73594513

[b]SINTEF Building and Infrastructure, Box 4760 Sluppen, NO-7465 Trondheim, Norway, E-mail: tore.myrland.jensen@sintef.no

Abstract

This study focuses on the ductility of lightweight aggregate concrete (LWAC) in compression. For practical purposes, the well-known brittleness of LWAC compared to normal density concrete has limited the use of the material. Demands for energy dissipation and/or a controlled behaviour after failure may exclude LWAC as the preferred material, while an increase of the ductility in the compression zone in bending is made possible by employing closed links and/or fibre reinforcement. An experimental programme was set up, which consists of eight over-reinforced concrete beams subjected to four-point bending in order to study the ductility. The LWAC had a mass density of approximately 1800 kg/m^3, with a compressive strength of approximately 35 MPa. Four different configurations of the beams were investigated, only with LWAC in the compression zone, closed links with a spacing of 100 mm, 1% of steel fibre reinforcement and a combination of closed links and steel fibres. The pre-peak behaviour was approximately the same for all configurations, and as expected, the beams with only LWAC had a very brittle response after peak load. The other beams had different post-peak responses, but all were able to carry the load with quite large deflections after maximum loading. Moreover, the combination with both fibres and links demonstrated highly ductile behaviour.

Keywords: bending tests, confinement, ductility, lightweight aggregate concrete, steel fibre

1 Introduction

Lightweight aggregate concrete (LWAC) has been used as a construction material for many decades, with the main objective for using LWAC normally being to reduce the dead weight of structures. Thus, with a low weight, the dimensions of the foundations in buildings can be reduced in areas with low bearing capacities, while the inertia actions are reduced in seismic regions, thereby enabling an easier handling and

[1] Corresponding author. Tel.: +47 73594513
E-mail address: jan.overli@ntnu.no

transportation of precast elements. Even with the major advantage of a reduced weight and the high strength-to-weight ratio of the material compared to conventional concrete, the use of LWAC is still limited as a mainstream construction material in the building industry. However, for large and advanced structures such as high-rise buildings, bridges and offshore structures, it has been applied with great success [1-5]. Other advantages of LWAC compared to normal weight concrete are its improved durability properties, fire resistance and low thermal conductivity [6-10].

The major disadvantage of LWAC is the brittleness in compression at the material level compared to normal density concrete. Adequate strength, which can easily be fulfilled with lightweight concrete, is not the only required design criterion, as in overload situations an adequate ductility is essential for safety. Ductility is defined as the ability of individual structural members or entire structures to sustain significant inelastic deformations after achieving peak load without a significant loss in the capacity prior to failure. This is of great importance in the redistribution of forces, and is also a major consideration in the design of structures in seismic areas. The limited post peak behaviour of LWAC can help explain the limited use of the material, and requests for energy dissipation and/or controlled behaviour after peak load can therefore exclude LWAC as the preferred material.

It is well known that confinement increases the ductility of concrete as well as enhancing the concrete strength. Additionally, an active confinement from external stresses is more effective than a passive confinement, which is mobilized by an opposing transverse deformation from the Poisson effect. In reinforced concrete, the passive confinement from transverse reinforcement is the most common, and numerous researchers have investigated the effect of ordinary transverse steel reinforcement and the effect of adding fibres on the confinement in normal density concrete, both experimentally and theoretically [11-15]. For lightweight aggregate concrete, similar effects have been reported [16-18], and the effect of confinement is also taken into account in design codes for concrete structures [19]. Nevertheless, most studies on confinement focus on columns and cylinders that have only been subjected to uniaxial loading [20-22]. The flexural behaviour of LWAC beams with a focus on ductility has been reported, but only on under-reinforced beams [23-27].

This study focuses on the ductility in compartment type of structures of reinforced lightweight concrete. Examples in which LWAC will be economically feasible and advantageous are floating offshore structures and temporary floating ground-based structures, such as LNG terminals. A major consideration in such structures is to avoid an uncontrollable leakage in the compartments. Consequently, the compartments are post-tensioned to control the cracking in service life. Preliminary studies of rectangular compartment structures subjected to horizontal excitation from earthquakes indicate that such stiff box structures have to resist the dynamic in-plane forces more or less elastically without any significant energy dissipation in order to maintain structural integrity and avoid uncontrollable leakage in the compartments. When the structure is subjected to vertical excitation, particularly when the continuous top slab is carrying heavy equipment, the structure may be subjected to high g-forces with bending moment reversals if the response is elastic. The maximum acceleration and dynamic forces may be significantly reduced provided that the structure has a sufficient energy dissipation ability. The energy dissipation in flexure is primarily related to the yielding (and yielding reversal) of the reinforcement, although the stress-strain characteristics of the concrete in compression play an important role in limiting the amount of yielding possible before the break-down of the plastic zones. For this reason, the effect of confinement in the compression zone is of great importance.

The main objective in this study was to investigate the passive confinement effect of closed links and/or steel fibres on the ductility in LWAC structures. An experimental programme was set up, which consisted of eight concrete beams subjected to four-point bending. Four different configurations of the beams were investigated to study the response of only LWAC in the compression zone, steel fibre reinforcement, stirrups and a combination of steel fibres and stirrups. The influence of the concrete compressive characteristics on the amount of reinforcement yielding was more pronounced in structures subjected to a combined bending moment and axial force. Instead of introducing an axial force by post-tensioning the beams, they were heavily over-reinforced to focus on the compressive behaviour.

This experimental programme is considered a first step in investigating the ductility of LWAC structures, and only static loading was considered, even though repeated loading is very important to assessing structural integrity in seismic areas. In general, the confinement and ductility of LWAC are well documented

in the literature. However, there is a limited amount of information concerning the ductility of over-reinforced LWAC structures in bending or structures subjected to a combined bending and membrane action.

2 Experimental programme

2.1 **Set-up**

The test programme was designed to study the ductility enhancement in heavily over-reinforced lightweight aggregate concrete beams provided by steel fibres and steel confining transverse reinforcement. The main focus was on the ductility in the compression zone; thus, the beams were heavily reinforced to ensure a bending failure in the compression zone of the cross section before the tensile reinforcement yielded.

The experimental programme consisted of eight simply supported concrete beams, which were tested in flexure under a four-point loading system, see Fig. 1. Hence, the central part of the beam was in pure bending mode, which was the main focus of this work. The free span between the supports was 3.6 m, and two concentrated loads were symmetrically applied at a distance of 0.8 m. Four different configurations of the LWAC beams were investigated to study the response. Two beams with only LWAC were considered as the reference beams (Beam 1), two beams had steel fibres (Beam 2), and two had stirrups (Beam 3), whereas the final two beams had a combination of closed links and steel fibres (Beam 4). The two beams in each configuration were identical, but made from different batches.

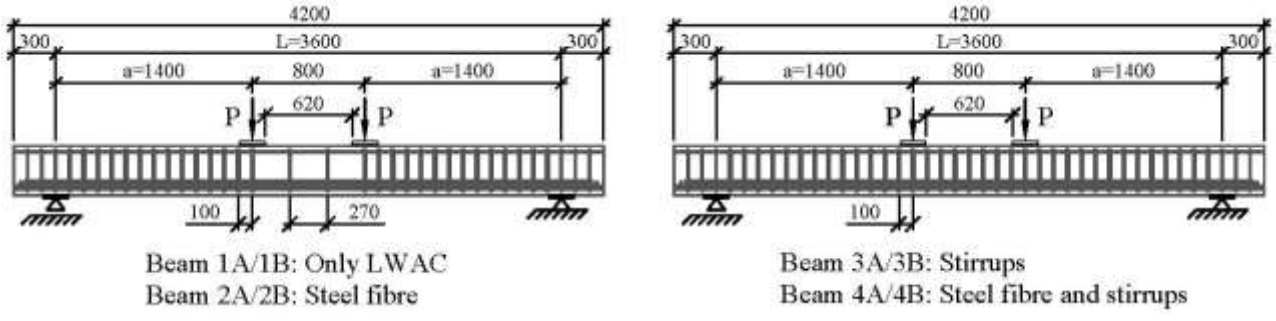

Fig. 1: Loading arrangement, confinement configurations and dimensions (in mm)

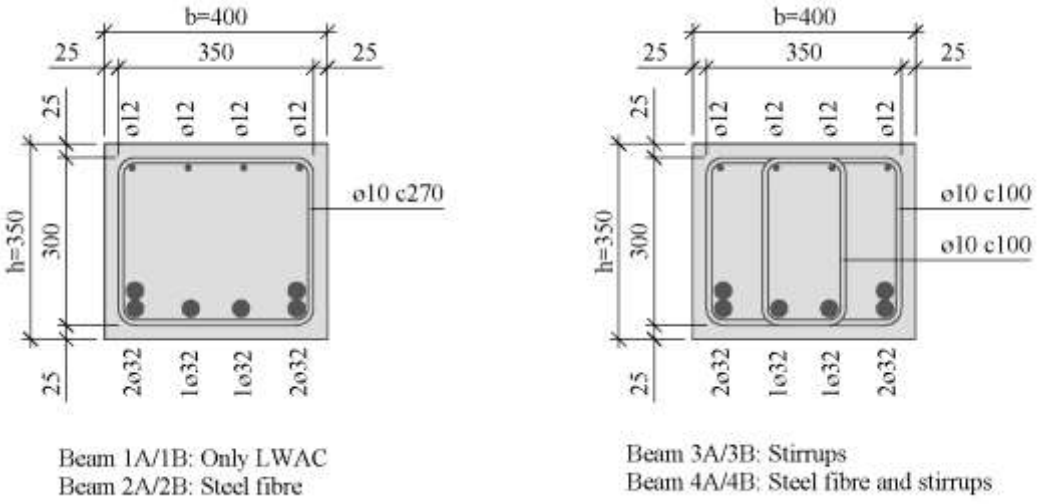

Fig. 2: Reinforcement layout at mid span and dimensions (in mm)

The cross sections in the beams were rectangular, 400 mm wide and 350 mm deep. The beams were designed to be over-reinforced, so that the longitudinal tensile reinforcement would not yield at failure. To help achieve this, six deformed bars with a diameter of 32 mm were provided. As seen in Fig. 2, they were arranged as four bars in a bottom layer and bundles of two bars on each side. In the compression zone, four bars with diameter 12 mm were placed in one layer, and in order to ensure enough anchoring capacity, a transverse horizontal bar with a diameter of 32 mm was welded onto the bottom layer of the tensile reinforcement at the ends of the beams.

The transverse reinforcement consisted of 10 mm diameter deformed bars bent into closed stirrups, while the concrete cover to the stirrups was 25 mm. The aim of this work was to study the ductility in compression; therefore, in the shear spans between the load point and the support, all beams were provided with stirrups with a spacing of 100 mm to ensure flexural failure. Both external and internal stirrups were used in each section to avoid shear failure. For beam types 3 and 4, which were designed to investigate the influence of stirrups on ductility, the same combination of external and internal stirrups with a spacing 100 mm was used in the flexural zone between the two concentrated loads. In beam types 1 and 2, only two outer stirrups were placed in the flexural zone to help avoid the buckling of longitudinal compression reinforcement, and can be considered spreader bars. These two stirrups only had a minor influence on the result, i.e. there was no effective confinement effect due to a large centre distance of 270 mm.

2.2 **Materials and mix proportions**

The LWAC in the project was designed and prepared in-house. To produce the concrete, a lightweight expanded clay aggregate, commercially known as LECA, was used to achieve the desired density of the LWAC. The project aimed for a mean compressive strength of ~ 35 MPa and a density of the LWAC of ~1800 kg/m^3. The concrete mix is given below in Table 1. The mix was the same for the A and B beams in each configuration, except for Beam 2, in which a minor change in the mix was necessary due to a different sand supplier. The LECA, including both 2-4 and 4-8 mm, had particle densities of 670 kg/m^3 and 1452 kg/m^3 , respectively. To improve the paste/cement and fibre/concrete bonds, the mix contained a silica fume of 9% by weight of the cement. In addition, limestone powder was added to avoid segregation, and the sand had a high content of fines to help increase the workability and stabilize the concrete. For beams with steel fibres, Dramix 65/60 was used, which is a cold drawn wire fibre of bright steel with hooked ends and a length of 60 mm. The tensile strength of the fibres was 1000 MPa, and the fibre content was 78 kg/m^3, which corresponds to an amount of fibres of 1% by volume of concrete.

The moisture content and the absorbed water in the LECA were measured, which was necessary input when adjusting the concrete mix. After the casting of beam type 1, there were some uncertainties about the moisture distribution in the LECA. The two fractions of LECA were then homogenized in a drum and sealed in plastic bags. Thus, the LECA in each concrete batch had almost the same moisture content.

Table 1:
Concrete mix proportions for LWAC

Constituent	Weight [kg/m^3]			
	Beam 1	Beam 2	Beam 3	Beam 4
Cement (CEM I)	430.0	428.1	428.5	428.8
Silica fume	38.7	38.5	38.6	38.6
Limestone powder	8.6	8.6	8.6	8.6
Water (free)	192.8	192.0	192.1	192.3
Absorbed water	6.9	2.3	6.5	2.3
LECA 2-4 mm	148.9	179.4	173.5	176.3
LECA 4-8 mm	198.6	239.2	236.9	235.1
Sand 0-8 mm	708.8	774.9	767.8	781.8
Superplasticizer	7.7	4.7	6.2	4.7

The mixing was done using a 0.8 m^3 laboratory mixer. First, cement, silica fume, LECA and sand were mixed for approximately 2 min. Water was then added, and the superplasticizer was continuously added and

adjusted during mixing until the desired workability of the concrete was achieved. Lastly, steel fibres were carefully spread in the mixer to help achieve a uniform distribution of the fibres in the concrete.

2.3 **Mechanical properties**

Mechanical properties were obtained for the LWAC for the different batches. For each beam, six cylinders with a diameter of 100 mm and a height of 200 mm were cast to find the compressive strength, f_{lcm}, and the density of LWAC, both after 28 days (water stored cylinders) and on the day of testing (cylinders stored together with the beams). The strength and the density were found according to the standards in [28] and [29], respectively. For half the beams (beams 1B, 2B, 3B and 4B), the modulus of elasticity, E_{lcm}, was found by following the procedure in [30]. Table 2 presents the obtained mean mechanical properties from tests from the same day as the testing of the large beams.

Table 2:
Mechanical properties for different mixes

Beam no. and configuration	f_{lcm} (MPa)	E_{lcm} (GPa)	Density, ρ_l (kg/m^3)	Oven-dry density, ρ (kg/m^3)	m
1A: Only LWAC	36.9	-	1759	1560	1.09
1B: Only LWAC	39.7	19.0	1812	1610	-
2A: Steel fibre	34.9	-	1818	1620	1.10
2B: Steel fibre	39.6	18.3	1881	1680	-
3A: Stirrups	34.5	-	1798	1600	1.10
3B: Stirrups	33.5	20.0	1822	1620	-
4A: Steel fibre + stirrups	27.7	-	1783	1580	1.09
4B: Steel fibre + stirrups	40.4	18.0	1827	1630	-

The variation in compressive strengths in each beam configuration can be explained in part by differences in density, as the beams with the largest density also had the largest strength. However, for beam type 3 it was the opposite result, though here the differences in density and strength were smaller than for the other beam types. From Table 2, it can be seen that the compressive strength varied quite a bit considering the equal w/b-ratio of the mixtures. The variation was large, especially for beams 4A and 4B. Compared to the other beams, the batch for beam 4A had a bad workability which influenced the compaction. The variation in the

degree of compaction, i.e. the air content, due to the fibre content, was also expressed by the variation in the density of the hardened concrete.

From one batch for each of the beam types (beams 1A, 2A, 3A and 4A), the compressive stress-strain relationships were found based on three cylinders with a height of 280 mm and a diameter of 100 mm, following the testing procedure described in [31]. Fig. 3 presents the obtained mean stress-strain relationship for the LWAC with 0% and 1% of steel fibre, respectively. The stress-strain relationship is also plotted in the diagram according to Eurocode 2 (EC2) [19]. The fibres had an effect on the descending part of the relationship, which is in agreement with results reported in the literature [32-34]. In general, fibres increase the compressive strength [18, 34, 35], although decreases in strength have also been reported [36]. The influence of fibres strongly depends on the amount, dispersion and type of fibre, aggregate type and size, workability of the concrete and degree of compacting achieved. In this work, ductility was the primary focus, while the compressive strength was of minor interest.

In Table 2, the parameter *m* is also given. This is the relationship between the secant modulus at 60% of the failure load and the secant modulus at failure. It is a measurement of the ductility and degree of the pre-peak non-linearity of the stress-strain relationship. As expected for LWAC, the parameter is quite small, and is confirmed in the stress-strain relationships in Fig. 3. The obtained Poisson's ratios at 40% of the ultimate capacity varied between 0.21 and 0.23, and no effects of fibres were observed for the ratio. This can partially be explained by the low load level and the long fibres, which were of the same magnitude as the diameter of the cylinder.

The beams in this project were over-reinforced. In order to be able to evaluate the results, compare the strains from the experiments with calculations and verify that the beams were over-reinforced, deformed bars with diameters 10 and 32 mm were tested according to [37] to help characterize the properties. The bar with a diameter of 10mm had an almost perfect linear-ideal plastic behaviour with a yield stress of 549 MPa and a modulus of elasticity of 199 GPa. The bars with a diameter of 32 mm had a more non-linear behaviour with an initial yielding at 442 MPa, before reaching a plastic yield stress of 565 MPa at a strain of 3.75 mm/m.

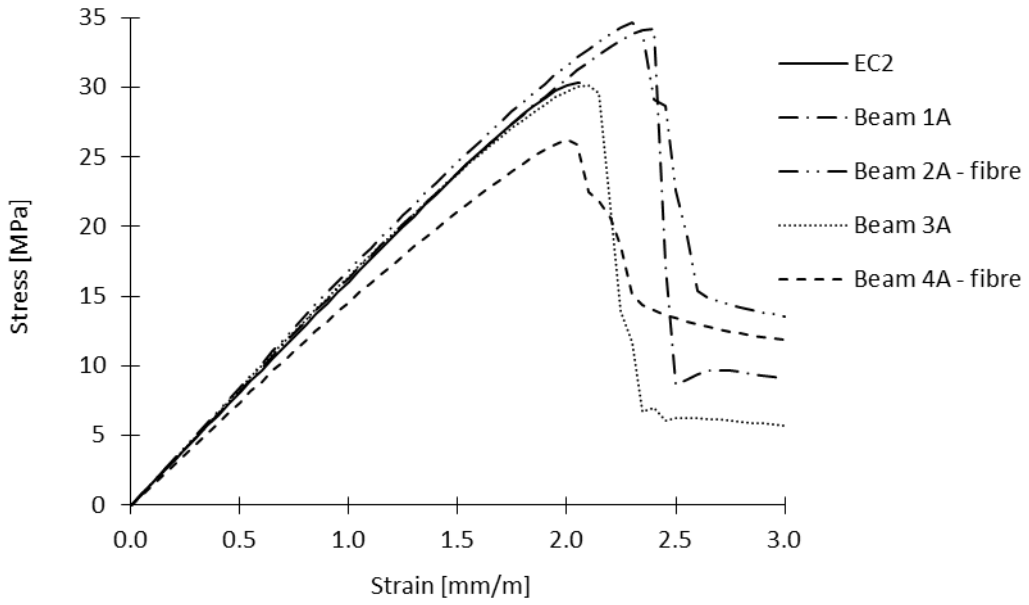

Fig.3: Stress-strain relationships for lightweight aggregate concrete

2.4 **Instrumentation and test procedure**

The beams were suitably instrumented to measure displacements and strains, see Fig. 4 and Fig. 5. Deflections of the beams were measured at the mid span and at the load transfer points by three vertical linear variable differential transformers (LVDT), IT5-IT7. To help capture the concrete strains, four LVDTs were placed horizontally at the top and bottom levels on both sides of the cross section, IT1-IT4. They measured the longitudinal displacements over a distance of 0.5 m, and six strain gauges were used to measure the steel strains. In the longitudinal direction, two gauges were mounted on the two central reinforcement bars on both the top and bottom, SG1-SG4. Since validation of the confinement effect was one of the main objectives in this study, two strain gauges were used in the horizontal direction of the shear links at the top, SG5-SG6.

The load was applied by a 1000kN servo-controlled hydraulic actuator, and distributed to the LWAC beam by a steel beam (equalizer beam) with two rolled supports, see Fig. 4. At an initial stage, the beams were preloaded with a very small load to remove any slack in the system. The load was then released, all instruments were zeroed and the beams were loaded at a rate of 1.0 mm/min. Up to a load level of 66.7 kN, the loading was applied in intervals of 16.7 kN, whereas above 66.7 kN, the intervals were doubled to 33.3 kN. At each load level there was a 5 min. break to study the formation of cracks, and after reaching the load

for the spalling of the concrete cover, the beams were continuously loaded. All displacement, strain and load readings were automatically logged with a rate of 0.5 Hz.

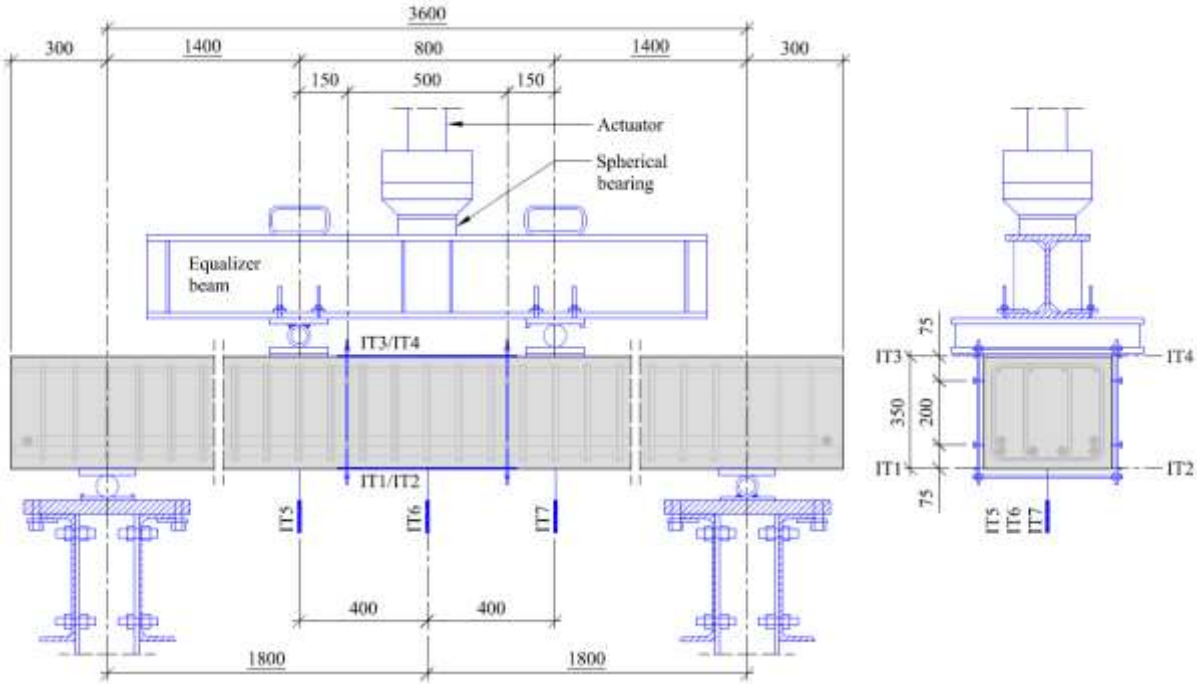

Fig. 4: Loading arrangement and instrumentation (dimensions in mm)

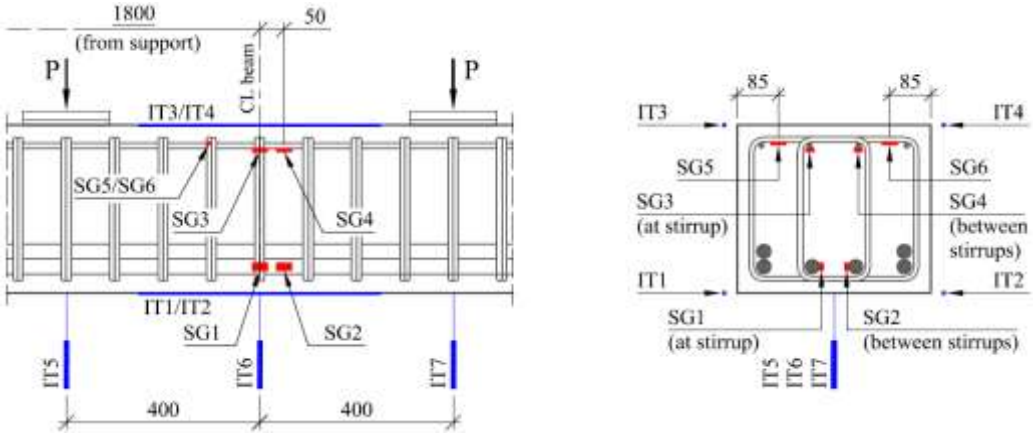

Fig. 5: Instrumentation of beams with strain gauges (SG1 to SG6) and LVDTs (IT1 to IT7) (dimensions in mm)

3 Results

3.1 **Load-displacement relationship**

In order to investigate and describe the response of the tested beams, reference will be made to the characteristic bending response of over-reinforced LWAC beams, both with and without confinement. This

is illustrated in Fig. 6, including two load levels of special interest. The spalling load, P_{spall} with a centre point deflection Δ_{spall}, is identified as the peak load when horizontal cracking in the compression zone occurs. Due to a deformation-controlled testing system and confinement effect, a peak load, P_{peak} with centre point deflection Δ_{spall} , represents a second maximum load level obtained after the spalling load. The response can best be described by five stages:

1. Before concrete cracks, 0-A.
2. Linear response for a cracked cross section, A-B.
3. Non-linear response, B-C, before reaching the compressive capacity (strain limit) of the beam, which initiates the spalling in the compressive zone.
4. Very brittle behaviour for beams with only LWAC, C-F, as well as for beams with confinement in the compressive zone, a redistribution of stresses that involves the spalling of the concrete cover, reaching a second peak load, C-D.
5. With confinement, a ductile post–peak behaviour, D-E.

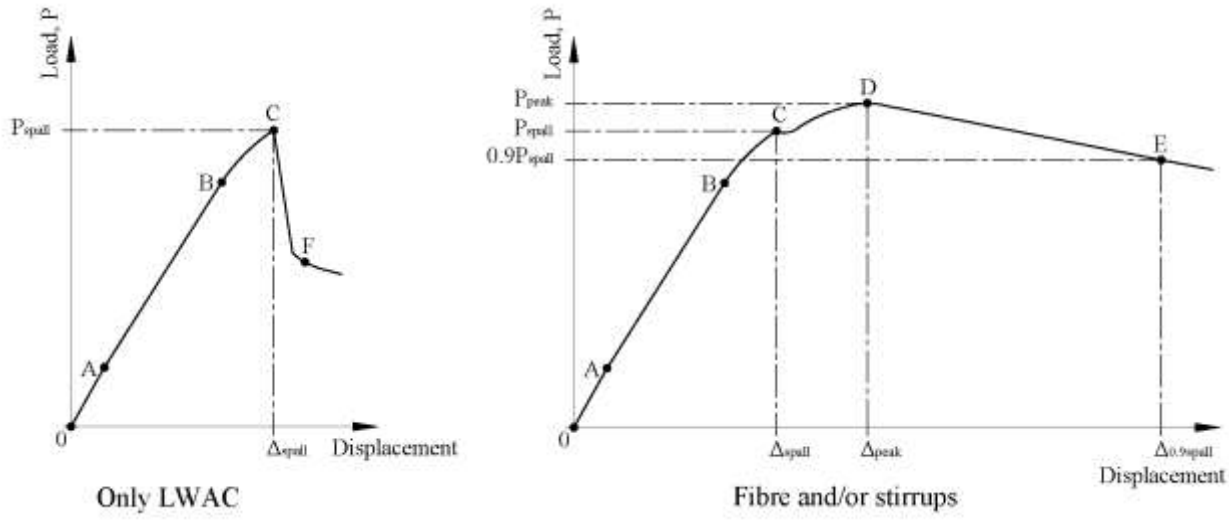

Fig. 6: Schematic load-displacement behaviour of over-reinforced LWAC beams, both with and without confinement

The load-displacement curves for the centre point are given in Fig. 7 for the eight beams. As expected, beams with only LWAC, beams 1A and 1B, had a very brittle response after reaching its maximum capacity (load at spalling). The responses for the beams demonstrated the strong influence of the different

confinement configurations on the behaviour at and after spalling. Before reaching the spalling load, there was no significant influence from the different configurations. However, some increased elastic bending stiffness can be identified by introducing confinement into the compression gradient zone.

Beams with fibre, beams 2A and 2B, had a ductile response. After the initiation of spalling, the load capacity was levelled out with no increase in capacity. In the post-peak behaviour, which included a descending branch in the load-displacement response, the two beams had different responses. In the casting of the beams, there were differences in the workability of the concrete which influenced the fibre distribution and orientation. Nonetheless, even if the registration of distribution and fibres was not performed, this is an indication of the importance of the fibre content on the compressive ductility.

Beams with shear reinforcement but no fibres, beams 3A and 3B, exhibited a very clear unloading after the first peak load, which was associated with the spalling of the concrete cover in the compression zone. However, the shear links were able to maintain a cross section, and after some redistribution of the stresses, a second peak point can be identified. This can clearly be seen in Fig. 7, where loads and displacements for each beam are normalized with respect to the spalling load and the corresponding spalling displacement. After the peak point, the beams had a ductile response analogous to the beams with fibre.

The beams with fibre and stirrups, beams 4A and 4B, had a very ductile behaviour. They also experienced a significant increase in capacity from a load at spalling to a peak load (approximately 10%). Thus, the confinement effect from fibres and stirrups increased the compressive strength in addition to an increased ductility. After achieving peak load, the beams were able to maintain a high load level with only a slight descending gradient.

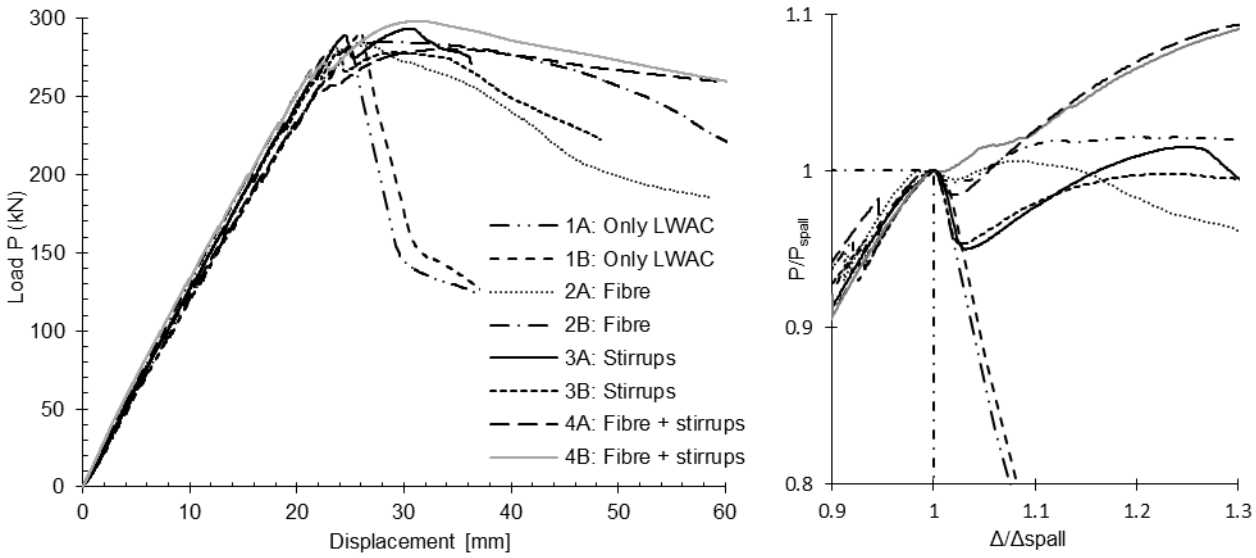

Fig. 7: Load-displacement plots

Table 3:
Experimental results

Beam: Configuration	P_{spall} (kN)	P_{peak} (kN)	P_{peak}/P_{spall}	Δ_{spall} (mm)	Δ_{peak} (mm)	$\Delta_{0.9,spall}$ (mm)	$\varepsilon_{c,spall}$ (10^{-3})	$\varepsilon_{s,spall}$ (10^{-3})	$\varepsilon_{c,peak}$ (10^{-3})	$\varepsilon_{s,peak}$ (10^{-3})	$\varepsilon_{c,0.9,spall}$ (10^{-3})	$\varepsilon_{s,0.9,spall}$ (10^{-3})
1A: Only LWAC	280.9	-	-	24.8	-	-	-2.98	2.11	-	-	-	-
1B: Only LWAC	291.2	-	-	25.9	-	-	-2.93	2.31	-	-	-	-
2A: Steel fibre	281.1	282.9	1.01	23.9	30.5	37.2	-2.95	2.25	-3.82	2.51	-10.9	5.5
2B: Steel fibre	279.0	284.9	1.02	23.1	29.5	52.1	-2.77	2.20	-5.23	2.48	-19.3	8.5
3A: Shear links	289.2	293.5	1.01	24.5	26.0	41.0	-2.66	2.11	-5.27	2.78	-9.3	5.4
3B: Shear links	279.0	278.4	1.00	23.9	28.8	39.5	-2.74	2.09	-5.48	2.63	-13.4	6.8
4A: Shear links + steel fibre	253.1	280.5	1.11	22.0	34.2	100.7	-2.49	1.95	-7.32	2.91	-52.1	22.0
4B: Shear links + steel fibre	271.5	298.3	1.10	22.6	31.4	79.9	-2.83	1.86	-5.93	2.68	-36.1	14.2

3.2 **Failure mode and ultimate strength**

Typically, the governing failure mode for all beams was bending failures for over-reinforced beams, as the failure and spalling of the concrete cover were initiated and identified when horizontal cracks occurred in the compression zone. Depending on the degree of confinement, Fig. 8 shows the typical difference in the failure zone between different confinement configurations at peak load and after the spalling load was reduced to 90%. The reference beam with only LWAC had a total delamination of the compressive zone at peak load. Hence, the capacity of the beam was reached. For the beams with stirrups, the horizontal cracking was quite substantial at peak load, and the concrete cover above the stirrups was almost separated from the beam.

However, inside the stirrups, the concrete only experienced a minor cracking in the compressive zone and the beams were still able to carry the load. For the beams with fibre, there was only minor cracking at the peak load. The cross section remained much more intact and was able to maintain a high load level after the peak load. From the illustrations, it is clear that the size of the spalling zone in the longitudinal direction was typically limited by a distance of 620 mm between the fibreboards in the pure bending zone. Consequently, these plates worked as external confinement with respect to spalling, and with increased deformation after the peak load, failure zones started to develop. The zone for the beam without fibres was much more local and concentrated than with fibres, where the zone was wider and deeper.

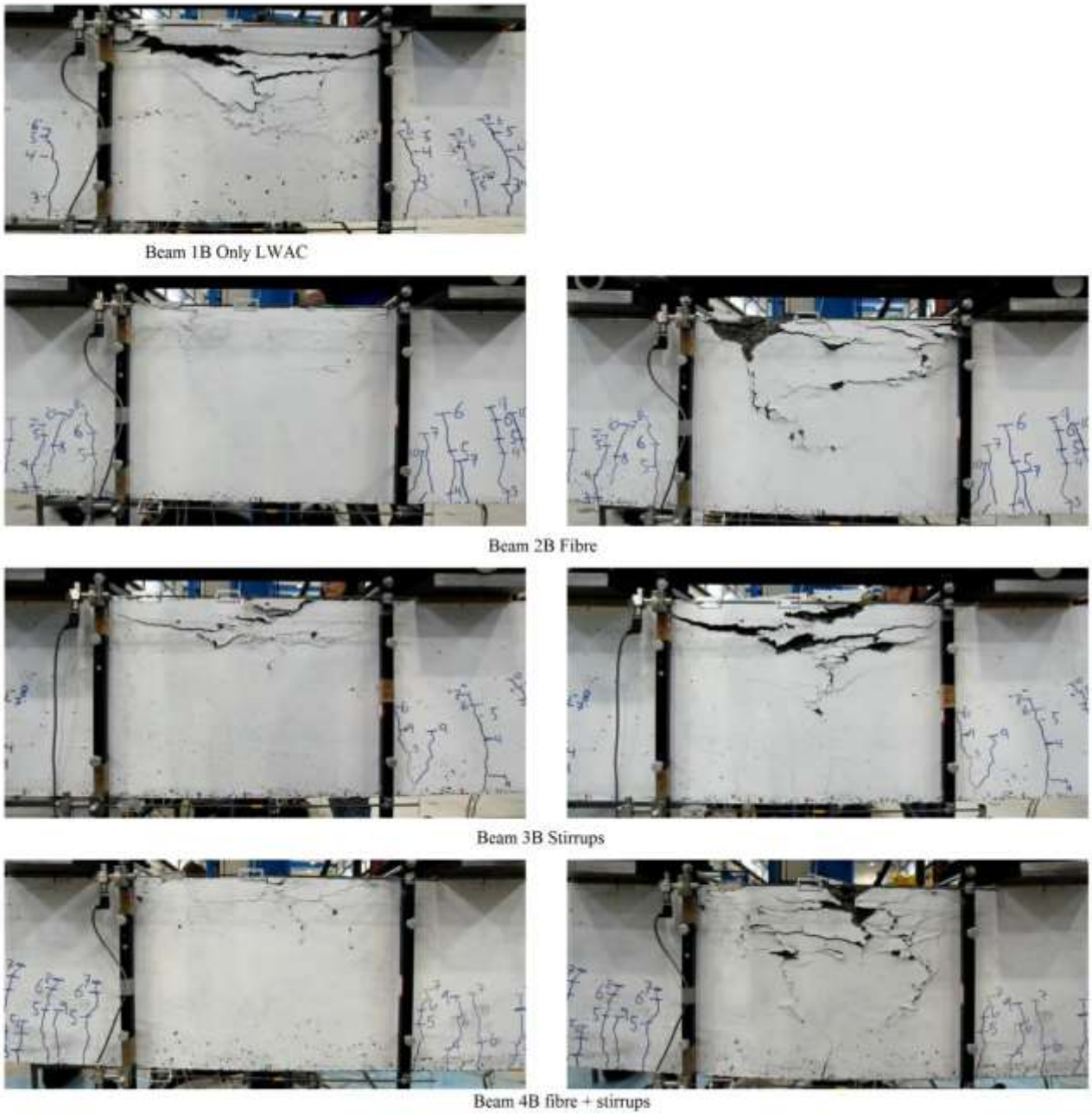

Fig. 8: Failure zone in beam at peak load (left) and at $0.9P_{spall}$ (right)

The recommendations in EC2 were employed so that the test results could be compared with the theoretical predictions of bending capacity. The theoretical values for spalling loads were calculated using the measured stress-strain relation for the reinforcement and the concrete, while the compressive strain at peak stress was calculated according to EC2 based on the oven dry density, ρ, of the LWAC, which was also in accordance with experiments from the cylinder tests. When comparing the spalling loads, the calculations considered the equivalent rectangular stress diagram for concrete in compression according to EC2, though the effect of different confinement in the compressive zone was not taken into account. This was in agreement with the experimental results, in which fibres and stirrups did not have any significant effect on the capacity at spalling and the stiffness before spalling. In Table 4, the theoretical predictions of the load capacity, P_{calc}, are given and compared with the test results, P_{spall}. In general, the agreement is good, and with the exception of beam 4B, the calculations slightly underestimate the capacity for beams with stirrups. For beams without stirrups, the buckling of compressive bars may have introduced an additional tensile stresses in the lateral direction, which could contribute to a premature spalling of the concrete cover, thereby helping to explain the overestimation in the calculations. Fig. 9 shows the influence of compressive strength on the ratio of test to calculated capacities at spalling, and with an increasing strength, the overestimation in calculated capacity also increased.

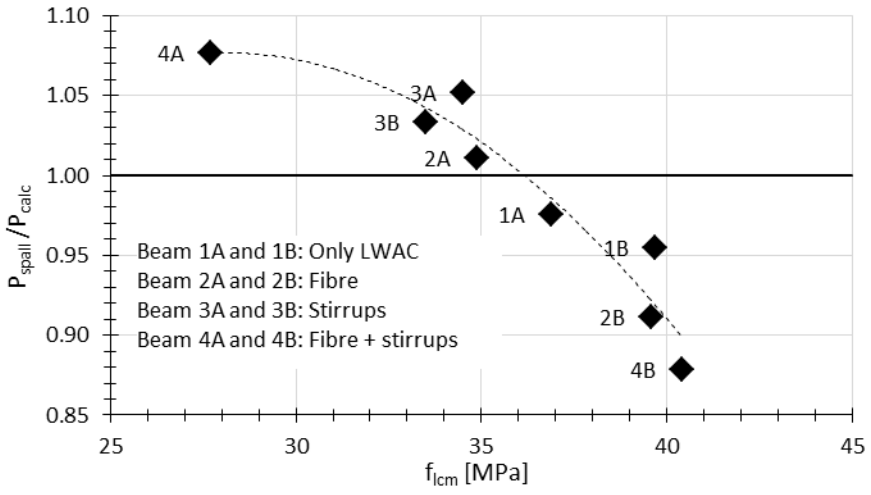

Fig. 9: Influence of compressive strength on the ratio of test to calculated capaities at spalling

3.3 **Concrete and steel strains**

The strain development during loading is shown in Fig. 10. Only the results from the first beam (A-beam) in each of the four configurations in the test series are presented, with similar responses obtained for the second

beams. In the figure, concrete strains are in the longitudinal direction of the beam on the top and bottom surfaces, reinforcement strains are in the top and bottom reinforcement and the transverse strains are in the horizontal part of the shear reinforcement close to the top surface. The strains in the reinforcement were measured locally with gauges, whereas the concrete strains were average strains over a distance of 0.5m. As a result, the reinforcement strains were more influenced by the location of cracks and the subsequent spalling, and the strain development confirmed the global load-displacement relationships. Up to the spalling load, the strains were not significantly influenced by the introduction of fibre and shear reinforcement. The beam with only LWAC had a very brittle response after spalling, while the beam with both fibres and shear links experienced an increase in bending capacity with large strains in the compressive zone. This increase in ductility can be explained by the effect of confinement. Due to the large compressive strains, the fibres and shear reinforcement were able to prevent some of the lateral expansion, which introduced small lateral compressive stresses that increased the compressive ductility. From the strains, it was possible to estimate the lateral expansion coefficient, defined as the relationship between the lateral- and the longitudinal strain. At load levels below the spalling load, the coefficient was approximately 0.20, which is a typical value for lightweight concrete. Between the spalling and the peak load, the coefficient increased to more than 0.3.

In Table 4, curvatures and reinforcement strains from the tests at spalling load are compared to the theoretical values obtained from the calculation of the load capacities, κ_{calc} and $\varepsilon_{s,calc}$ in Table 4. The test curvatures, κ_{spall} and κ_{peak}, were derived on the basis of the average measured strains in the tensile reinforcement, $\varepsilon_{s,spall}$ and $\varepsilon_{s,peak}$ in Table 3 and the concrete strains at the top surfaces, $\varepsilon_{c,spall}$ and $\varepsilon_{c,peak}$ in Table 3. With the exception of beam 4B, the compared values are in close agreement. The calculations overestimated the curvatures and the strains in the reinforcement, which can be explained in part by the assumption of no confinement effect from stirrups and fibre to the stress-strain relationship in the predictions. The obtained concrete compressive strains at spalling correspond with the ultimate compressive strain, ε_{lcu3}, from EC2 used in calculations.

The strain distributions in the cross section at spalling and at peak loads are illustrated in the front elevation for each beam in Fig. 11. Due to spalling, the strain gauges on the compressive reinforcement failed when approaching the peak load for Beam 1 and Beam 4, and no measurements were available. Moreover, strain

measurements up to P_{spall} showed a reasonable resemblance between strain gauges and LVDTs. Therefore, the strain distribution can be considered to be linear over the cross section and evenly distributed across the middle 500 mm of the beams. Strains in the reinforcement were local, while strains on the top and bottom surfaces of the beams represented average strains over a length of 500 mm. Loading above P_{spall} introduced a concentration of strains towards the middle of the span of the beam due to the formation of a plastic hinge region, which can be observed from beams 2A and 3A since the strains in the compressive reinforcement increased more than the average strain on the top surface from P_{spall} to P_{peak}. The response from the tensile reinforcement was elastic all the way up to the peak load for all beams. Hence, the beams can be characterized as over-reinforced. The compression reinforcement developed their full yield strength at peak load, and their contribution to the moment capacity was approximately 10%. The compression reinforcement also contributed to the ductility of the beams since the height of compression zone was reduced.

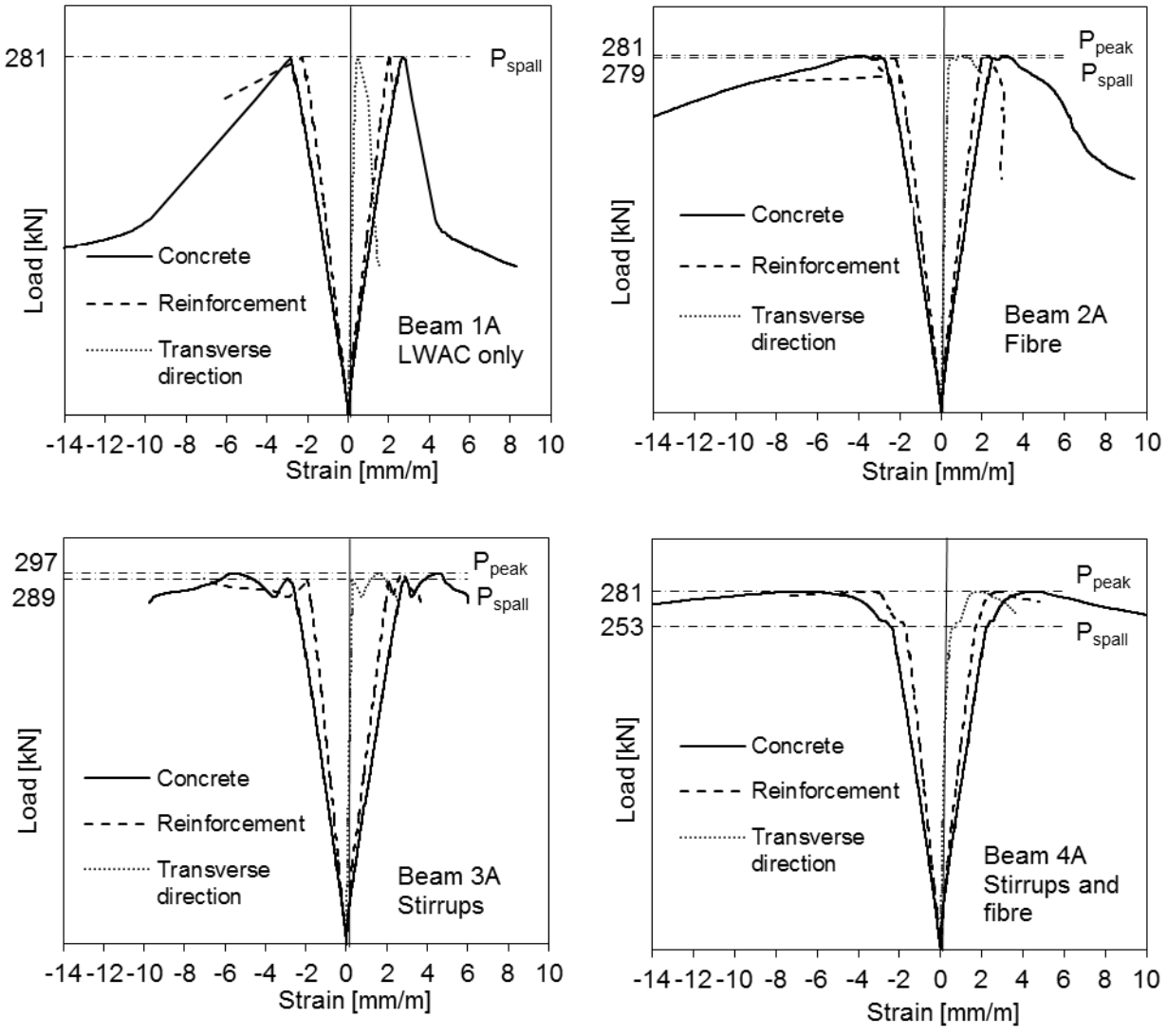

Fig. 10: Strain development for the four different configurations of beams

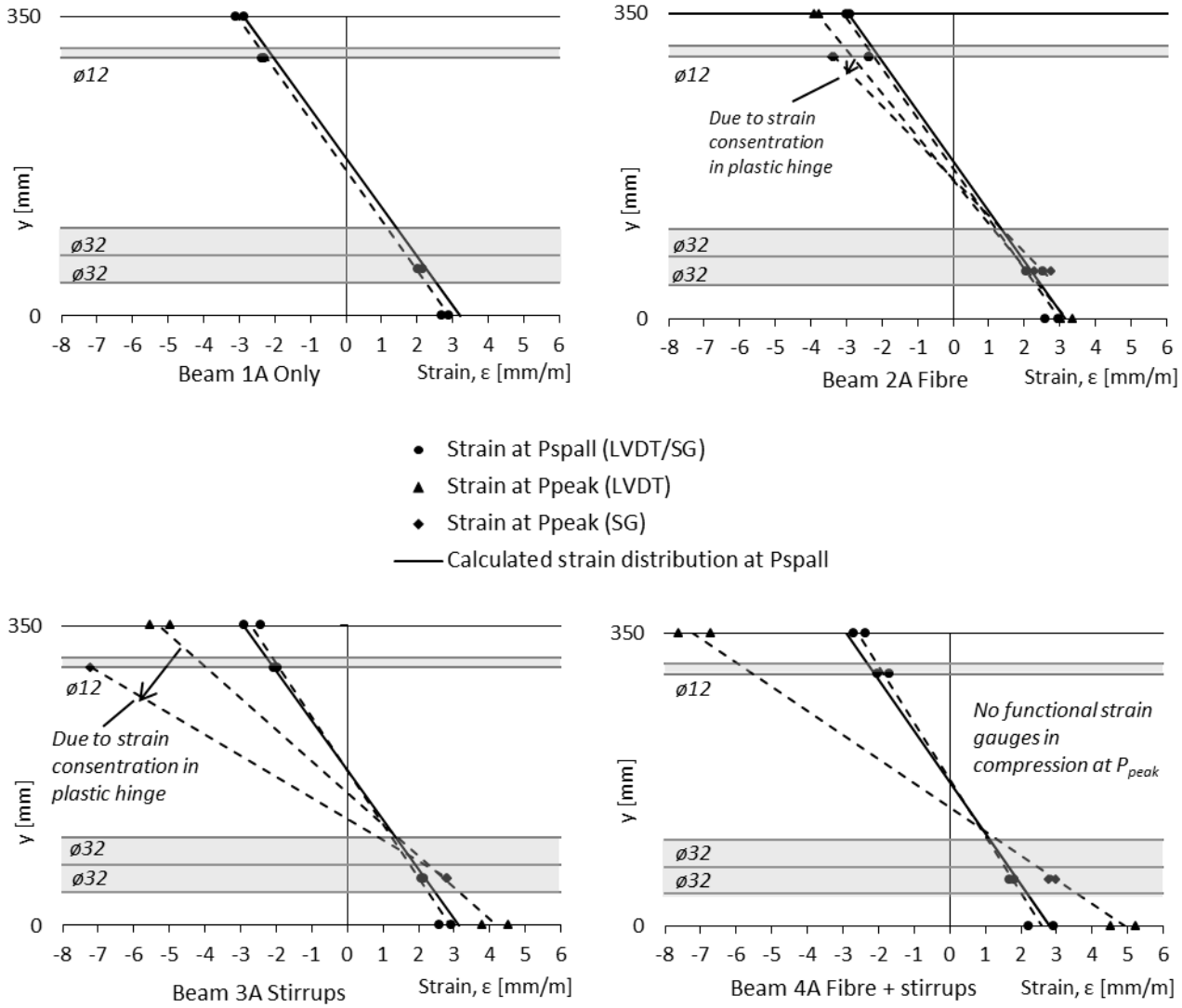

Fig. 11: Longitudinal strain distribution in cross section at spalling and peak load

Table 4:
Experimental and theoretical values

Beam: Configuration	P_{calc} [kN]	P_{spall}/P_{calc}	ε_{lcu3} (10^{-3})	κ_{spall} (mm^{-1})	κ_{peak} (mm^{-1})	κ_{calc} (mm^{-1})	$\varepsilon_{s,calc}$ (10^{-3})	$\kappa_{spall}/\kappa_{calc}$	$\varepsilon_{s,spall}/\varepsilon_{s,calc}$	$\mu_{\Delta,1}$	$\mu_{\Delta,2}$	μ_{E1}	μ_{E2}
1A: Only LWAC	288	0.98	2.89	17.0	-	17.4	2.31	0.98	0.91	-	-	-	-
1B: Only LWAC	305	0.96	2.94	17.5	-	18.0	2.45	0.97	0.94	-	-	-	-
2A: Steel fibre	278	1.01	2.95	17.3	21.1	17.4	2.26	0.99	0.99	1.09	1.56	1.32	2.28
2B: Steel fibre	306	0.91	3.00	16.6	25.7	18.3	2.47	0.91	0.89	1.25	2.26	1.62	3.69
3A: Shear links	275	1.05	2.93	15.9	26.8	17.3	2.25	0.92	0.94	1.25	1.67	1.59	2.07
3B: Shear links	270	1.03	2.95	16.1	27.0	17.3	2.21	0.93	0.94	1.23	1.65	1.65	2.65
4A: Shear links + steel fibre	235	1.08	2.91	14.8	34.1	16.3	1.97	0.91	0.99	1.56	4.57	1.95	7.26
4B: Shear links + steel fibre	309	0.88	2.96	15.6	28.7	18.2	2.48	0.86	0.75	1.39	3.54	1.76	5.67

3.4 **Ductility**

Ductility is the ability for a structural member to deform inelastically without any significant loss of strength. It can be measured at various levels in a structure, in the material, in a section, in an element or on global levels. The most common way of quantifying ductility is to employ a ductility index, which on a sectional level is often defined as the ratio of curvature at the crushing of concrete to that of the yielding of the reinforcement. In the seismic design in Eurocode 8, in which the formation of yield hinges is important, the local sectional ductility index is defined with a post-peak value of 85% of the maximum value in bending [38]. In this study, the beams were over-reinforced, meaning that the yielding of reinforcement cannot be used to find a ductility index. Instead, ductility indexes were defined based on the response at the spalling load, peak load and at a post-peak response at 90% of the spalling load.

Due to the traditional focus on the compressive strength of concrete, the definitions of ductility are often based on the stress-strain curve in compression. For the over-reinforced beams in this experiment, in which the structural ductility was directly related to the toughness in the compressive zone, an analogous evaluation can be made by investigating the ratio of plastic deformation and energy absorption to elastic deformation and energy absorption. The displacement ductility ratios were defined as $\mu_{\Delta,1}=\Delta_{peak}/\Delta_{spall}$ and $\mu_{\Delta,2}=\Delta_{0,9spall}/\Delta_{spall}$, where $\Delta_{0,9spall}$ is the centre point deflection at 90% of the spalling load. In the energy-based approach, the ductility was defined as the ratio between total energy and elastic energy, $\mu_{E1}=E_{tot1}/E_{elastic}$ and $\mu_{E2} = E_{tot2}/E_{elastic}$, as shown in Fig. 12.

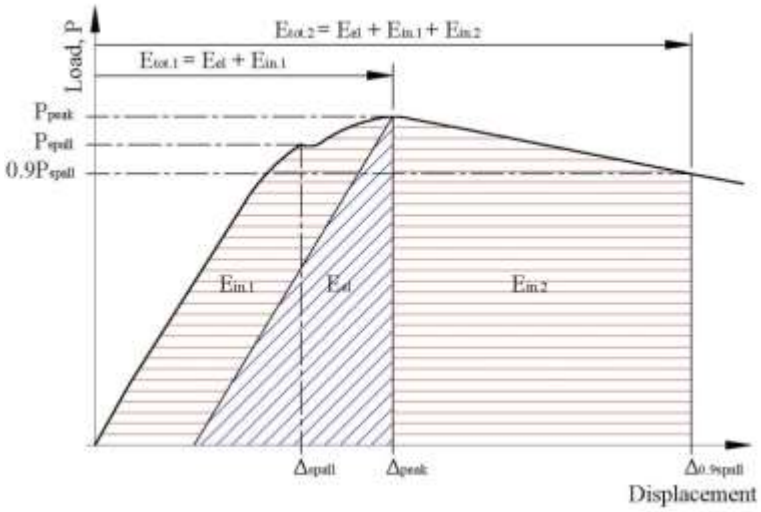

Fig. 12: Illustration of elastic, inelastic and total energy absorption

In Table 4, all the ductility ratios are given for the different beam configurations. The ratios defined at $0.9P_{spall}$ were at the same level for beams with either stirrups or fibre, while for the combination of stirrups and fibre, the ratio was approximately doubled. Thus, the effect of confinement reinforcement and fibres was an additive effect with respect to ductility in this test series. The large ductility for beams 4A/4B with fibre and stirrups was partly due to a significant increase in load capacity from the initiation of the spalling to the obtained peak load in combination with a very gradual descending branch of the deformation. The displacement and energy absorption after the peak load were also related to some local yielding of the tensile reinforcement within the plastic hinge region. Before reaching the peak load, the elastic deformations and energy absorption were primarily associated with elastic strain in the tensile reinforcement and in LWAC in the compressive gradient zone, respectively. Plastic deformations and energy absorption were primarily related to plastic strains in the LWAC, some yielding of the compressive reinforcement, as well as an internal friction between tensile reinforcement and LWAC. As a result, the ductility factors defined at peak loads did not vary much for the different confinement configurations.

3.5 **Displacement relationships within the plastic hinge region**

The rotational capacity of plastic hinge areas plays an important role in the analyses of ultimate load capacity and the ductility of continuous beams and frames. The different moment redistribution potential can be illustrated by comparing the displacement relationships at the mid span and at load points for the over-reinforced beams with the same reinforcement ratio in this study. For the beams in this study, the

reinforcement ratio was very high, and the plastic rotation capacity depended almost completely on the limited plastic strain of LWAC alone. Hence, the different displacement relationships at peak loads were only related to the different confinement configurations in the compressive gradient zones. Fig. 13 presents a schematic diagram of how the relationships between displacements at mid span and at load points are theoretically limited by a lower limit of 1.066 and an upper limit of 1.286. The lower limit assumes linear elastic material properties and a constant bending stiffness in the beam. However, lower values appear before spalling due to non-linear stress-strain relationships in the compressive zone between the load points, which gives a distributed reduced stiffness in the bending zone. The upper limit represents a theoretical model with a locally concentrated plastic hinge, with a much lower bending stiffness than the rest of the beam.

Fig. 14 presents the test results of the ratio of mid span to load point displacement, $\Delta_{IT6}/\Delta_{IT5,IT7}$, with respect to mid span displacement, Δ_{IT6} , and the load response is also given in the figures. At load levels below spalling the ratio is typically in the range between 1.04 – 1.05, which is close to the expected values, whereas after spalling the ratio increased. For beams with only LWAC, beams 1A and 1B, there was a pronounced increase just after spalling before levelling out with a ratio of approximately 1.16, and such a shape in the graph was in accordance with the formation of a very local plastic hinge. From Fig. 14, it can clearly be seen that the beams with fibres and/or stirrups had a much more gradual increase in the ratio after the spalling load. For this reason, the beams were able to activate a larger area during the formation of the plastic zone in the middle part of the beam, which is confirmed by the pictures of the failure zones in Fig. 8.

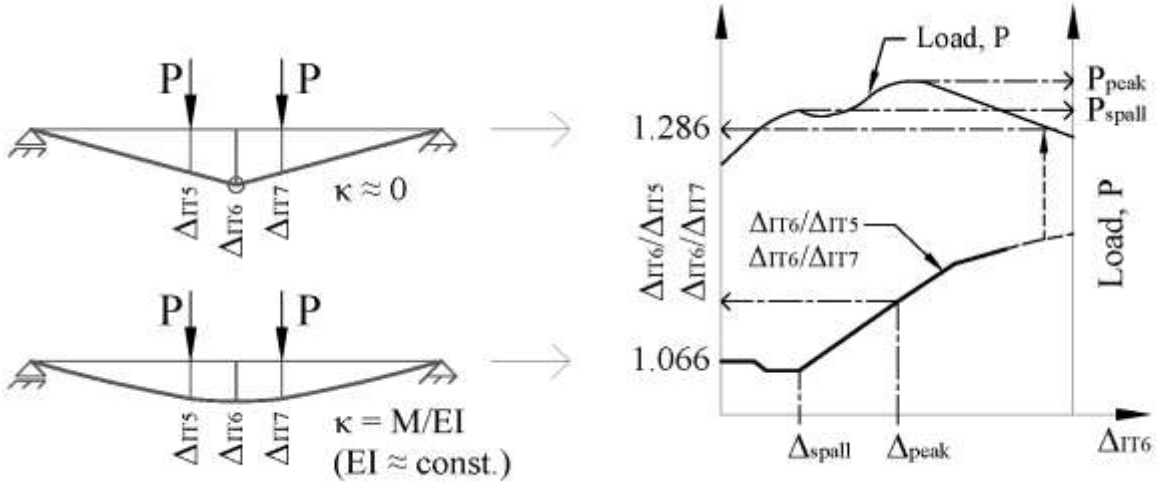

Fig. 13: Schematic relationships between displacement at mid span and at load points

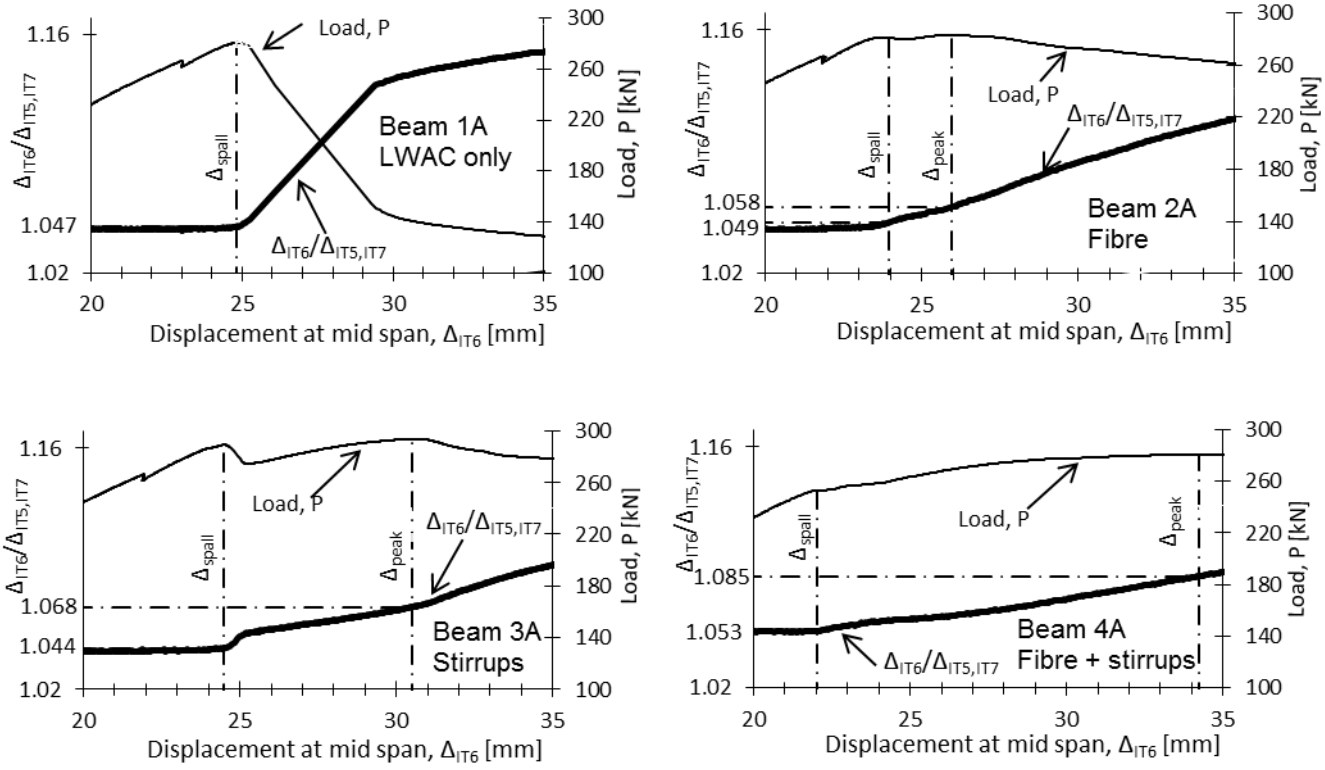

Fig. 14: Relationship between displacement at mid span and at load points

4 Conclusions

This study shows that the effects of introducing different types of passive confinement on the post-peak response are significant within the inelastic range of deformations. Furthermore, a considerable improvement of the structural performance regarding ductility and load-carrying degradation was obtained by employing steel fibre reinforcement, stirrups and a combination of fibre and stirrups. The results are promising, and indicate that LWAC has the potential to be consistent with the performance requirements for structural materials, including with regard to ductility in heavily reinforced and post-tensioned structures in seismic areas. The main findings in this study are:

- There was no significant influence from the different confinement configurations on the pre-peak response before the initiation of spalling and on the load capacity at spalling.
- The fibres introduced a softer transition at the spalling of the concrete cover, and there was no significant drop in the load response.

- The beams with only fibres had a ductile post-peak response, but displayed a large difference in the inclination of the descending branch, which may be explained by a different fibre distribution and orientation.
- Beams with only stirrups had a reduced capacity after the initiation of spalling, though before the confinement effect of the stirrups was activated and the load capacity increased again towards a peak load at the same level as the spalling load.
- Beams with both fibre and stirrups had a soft transition at spalling, but also a gradual and significant capacity increase of approximately 10% after the initiation of spalling. They had a very ductile post-peak response.
- The ductility index proved to be the same for beams with fibre or stirrups, and was almost doubled for beams with both fibre and stirrups.
- The effect of adding steel fibre reinforcement in the compressive gradient zone of full-scale, over-reinforced LWAC beams was much more pronounced regarding ductility than the effect achieved from tests of stress-strain relationships on cylinders with the same fibre reinforced LWAC.

Acknowledgements

The authors would like to acknowledge the financial support from COIN, the Concrete Innovation Centre, which is a centre for research-based innovation with funding from the Research Council of Norway and industrial partners, in addition to the assistance of L. Bakken, F. Lang, K. Sagosen and Ø. Rønningen for carrying out the experimental work as part of their master‘s theses [39, 40].

References

[1] ACI Committee 213. Guide for Structural Lightweight Aggregate Concrete (ACI 213R-03). American Concrete Institute. Farmington Hills, MI, United States: American Concrete Institute; 2003.
[2] fib bulletin 8. Lightweight Aggregate Concrete. Lausanne, Switzerland: International federation for Structural Concrete; 2000.
[3] Ingebrigtsen T. Stolma Bridge, Norway. Structural Engineering International. 1999;9:100-2.

[4] Melby K. Use of high strength LWAC in Norwegian bridges. In: Helland S, editor. International Symposium on Structural Lightweight Aggregate Concrete. Kristiansand, Norway: Norwegian Concrete Association; 2000.
[5] Haug AK, Fjeld S. A floating concrete platform hull made of lightweight aggregate concrete. Engineering Structures. 1996;18:831-6.
[6] Clarke JL. Structural Lightweight Aggregate Concrete: Taylor & Francis; 2002.
[7] Zhang M-H, Gjørv OE. Permeability of High-Strength Lightweight Concrete. ACI Materials Journal. 1991;88:463-9.
[8] Lo-shu K, Man-qing S, Xing-sheng S, Yun-xiu L. Research on several physico-mechanical properties of lightweight aggregate concrete. International Journal of Cement Composites and Lightweight Concrete. 1980;2:185-91.
[9] Neville AM. Properties of Concrete: Pearson Education; 2012.
[10] Jensen JJ, Hammer TA, Ophelm E, Hansen EA. Fire Resistance of Lightweight-Aggregate Concrete. In: Holand I, editor. International Symposium on Structural Lightweight-Aggregate Concrete. Sandefjord, Norway1995. p. 192-204.
[11] Attard MM, Setunge S. Stress-strain relationship of confined and unconfined concrete. ACI Materials Journal. 1996;93:432-42.
[12] Cheong HK, Zeng H. Stress-strain relationship for concrete confined by lateral steel reinforcement. ACI Materials Journal. 2002;99:250-5.
[13] Mander JB, Priestley MJN, Park R. Observed stress-strain behavior of confined concrete. J Struct Eng. 1988;114:1827-49.
[14] Sheikh SA, Toklucu MT. Reinforced concrete columns confined by circular spirals and hoops. ACI Struct J. 1993;90:542-53.
[15] Mander J, Priestley M, Park R. Theoretical Stress-Strain Model for Confined Concrete. J Struct Eng. 1988;114:1804-26.
[16] Balaguru P, Foden A. Properties of fiber reinforced structural lightweight concrete. ACI Struct J. 1996;93:62-78.
[17] Balendran RV, Zhou FP, Nadeem A, Leung AYT. Influence of steel fibres on strength and ductility of normal and lightweight high strength concrete. Building and Environment. 2002;37:1361-7.
[18] Campione G, La Mendola L. Behavior in compression of lightweight fiber reinforced concrete confined with transverse steel reinforcement. Cement and Concrete Composites. 2004;26:645-56.
[19] Standards Norway. NS-EN 1992-1-1:2004+NA:2008. Eurocode 2: Design of concrete structures - General rules and rules for buildings. Norway: Standards Norway; 2008.
[20] Kim Y-J, Harmon TG. Analytical model for confined lightweight aggregate concrete. ACI Struct J. 2006;103:263-70.
[21] Kosaka Y, Tanigawa Y, Hatanaka S. Lateral confining stresses due to steel fibres in concrete under compression. International Journal of Cement Composites and Lightweight Concrete. 1985;7:81-92.
[22] Mangat PS, Motamedi Azari M. Influence of steel fibre and stirrup reinforcement on the properties of concrete in compression members. International Journal of Cement Composites and Lightweight Concrete. 1985;7:183-92.
[23] Sin LH, Huan WT, Islam MR, Mansur MA. Reinforced lightweight concrete beams in flexure. ACI Struct J. 2011;108:3-12.
[24] Ahmad SH, Barker R. Flexural behavior of reinforced high-strength lightweight concrete beams. ACI Struct J. 1991;88:69-77.
[25] Ahmad SH, Batts J. Flexural behavior of doubly reinforced high-strength lightweight concrete beams with web reinforcement. ACI Struct J. 1991;88:351-8.
[26] Altun F, Aktaş B. Investigation of reinforced concrete beams behavior of steel fiber added lightweight concrete. Construction and Building Materials. 2013;38:575-81.
[27] Carmo RNF, Costa H, Simões T, Lourenço C, Andrade D. Influence of both concrete strength and transverse confinement on bending behavior of reinforced LWAC beams. Engineering Structures. 2013;48:329-41.
[28] Standards Norway. NS-EN 12390-3:2009. Testing hardened concrete - Part 3: Compressive strength of test specimens Norway: Standards Norway; 2009.
[29] Standards Norway. NS-EN 12390-9:2009. Testing hardened concrete - Part 7: Density of hardened concrete. Lysaker: Standards Norway; 2009.
[30] Skjølsvold O, Bakken N, Johansen E. KS 14-05-04-122: Bestemmelse av E-modul iht NS3676 - Losenhausen 5000kN trykkpresse. SINTEF Byggforsk: Betong og natursteinslaboratoriene; 2007.

[31] Skjølsvold O, Johansen E, Bakken N. KS 14-05-05-124: Arbeidsdiagram ved trykkbelastning, Losenhausen 5000kN trykkpresse. SINTEF Byggforsk: Betong og natursteinslaboratoriene; 2007.
[32] Düzgün OA, Gül R, Aydin AC. Effect of steel fibers on the mechanical properties of natural lightweight aggregate concrete. Materials Letters. 2005;59:3357-63.
[33] Shafigh P, Mahmud H, Jumaat MZ. Effect of steel fiber on the mechanical properties of oil palm shell lightweight concrete. Materials & Design. 2011;32:3926-32.
[34] Libre NA, Shekarchi M, Mahoutian M, Soroushian P. Mechanical properties of hybrid fiber reinforced lightweight aggregate concrete made with natural pumice. Construction and Building Materials. 2011;25:2458-64.
[35] Wang HT, Wang LC. Experimental study on static and dynamic mechanical properties of steel fiber reinforced lightweight aggregate concrete. Construction and Building Materials. 2013;38:1146-51.
[36] Kayali O, Haque MN, Zhu B. Some characteristics of high strength fiber reinforced lightweight aggregate concrete. Cement and Concrete Composites. 2003;25:207-13.
[37] Standards Norway. NS-EN ISO 15630-1. Steel for the reinforcement and prestressing of concrete - Test methods - Part 1: Reinforcing bars, wire rod and wire. Norway: Standards Norway; 2010.
[38] Standards Norway. NS-EN 1998-1:2004+NA:2008. Eurocode 8: Design of structures for earthquake resistance. Part 1: General rules, seismic actions and rules for buildings. Norway: Standards Norway; 2008.
[39] Bakken L, Sagosen KB. Ductility of lightweight aggregate concrete. Department of Structural Engineering: Norwegian University of Science and Technology; 2012.
[40] Lang FT, Rønningen Ø. Ductility of lightweight aggregate concrete. Department of Structural Engineering: Norwegian University of Science and Technology; 2012.

Figure captions

Fig. 1: Loading arrangement, confinement configurations and dimensions (in mm)

Fig. 2: Reinforcement layout at mid span and dimensions (in mm)

Fig.3: Stress-strain relationships for lightweight aggregate concrete

Fig. 4: Loading arrangement and instrumentation (dimensions in mm)

Fig. 5: Instrumentation of beams with strain gauges (SG1 to SG6) and LVDTs (IT1 to IT7) (dimensions in mm)

Fig. 6: Schematic load-displacement behaviour of over-reinforced LWAC beams, both with and without confinement.

Fig. 7: Load-displacement plots

Fig. 8: Failure zone in beam at peak load (left) and at $0.9P_{spall}$ (right)

Fig. 9: Influence of compressive strength on the ratio of test to calculated capaities at spalling

Fig. 10: Strain development for the four different configurations of beams

Fig. 11: Longitudinal strain distribution in cross section at spalling and peak load

Fig. 12: Illustration of elastic, inelastic and total energy absorption

Fig. 13: Schematic relationships between displacement at mid span and at load points

Fig. 14: Relationship between displacement at mid span and at load points